Atmos. Chem. Phys. Discuss., 10, 8995–9013, 2010
www.atmos-chem-phys-discuss.net/10/8995/2010/

Atmospheric Chemistry and Physics Discussions

This discussion paper is/has been under review for the journal Atmospheric Chemistry and Physics (ACP). Please refer to the corresponding final paper in ACP if available.

Empirical predictions of CCN from aerosol optical properties at four remote sites

A. Jefferson

Cooperative Institute for Research in Environmental Science (CIRES), University of Colorado, Boulder, CO, USA

NOAA Earth System Research Laboratory, Boulder, CO, USA

Received: 12 March 2010 – Accepted: 15 March 2010 – Published: 8 April 2010

Correspondence to: A. Jefferson (anne.jefferson@noaa.gov)

Published by Copernicus Publications on behalf of the European Geosciences Union.

Abstract

This study presents an empirical method to predict the CCN concentration as a function of percent supersaturation. The aerosol optical properties of backscatter fraction and single scatter albedo function as proxies for the aerosol size and composition in a power law relationship to CCN. This method is tested at four sites with aged aerosol: SGP (Oklahoma, USA), FKB (Black Forest, Germany), HFE (Hefei, China) and GRW (Graciosa, Azores). Each site represents a different aerosol type and thus demonstrates the method robustness and limitations. Good agreement was found between the calculated and measured CCN with slopes between 0.81 and 1.03 and correlation coefficients (r^2 values) between 0.59 and 0.67. The fit quality declined at low CCN concentrations in a region with higher data uncertainty.

1 Introduction

The highest uncertainty in estimates of climate forcing is the indirect forcing associated with clouds (Solomon et al., 2007). Clouds present a formidable challenge to parameterize their spatial variance, lifetime, albedo, precipitation and formation. The full characterization of aerosol activation into cloud droplets as a function of the percent super saturation is one such challenge. Calculation of aerosol activation to cloud condensation nuclei concentration (CCN) using Köhler's equation requires knowledge of the size-dependent aerosol composition. Because of the resource and computational intensive nature of these measurements and models, long term monitoring of aerosol size-dependent composition for different aerosol types and regions is not currently feasible. A widely used simplification of Köhler equation is the κ-Köhler model developed by Petter and Kriedenweis (2007), which uses a single parameter, κ, to relate the aerosol water activity and solute concentration. Several studies have a similar simplification of Köhler's equation or build upon the κ model by using proxies such as the aerosol hygroscopic growth (Good et al., 2009; Ervens et al., 2007; Petters et al.,

ACPD

10, 8995–9013, 2010

2009), soluble fraction and mixing state (Ervens et al., 2009), fraction of refractory material or organic composition (Shinozuka et al., 2009). Other empirical methods relate the CCN concentration to a power law fit using aerosol size and composition data or directly to the aerosol extinction (Gahn et al.,1995, 2006; Khvorostyanov and Curry, 2006; Andreae, 2009).

This study presents an empirical model of the CCN concentration from the aerosol optical properties. The model is a power law fit of the CCN data that uses the aerosol backscatter fraction and the single scatter albedo as proxies for the aerosol size and composition. The model fits empirical predictions of CCN for four regional sites from the US Department of Energy Atmospheric Radiation Measurement Climate Research Facilities (ACRF). Each of these sites represents a different aerosol type and shows both the robustness and limitations of this method in predicting CCN. The sites in this study are the Southern Great Plains, Oklahoma (SGP), the Murg Valley, Germany (FKB), Shouxian, China (HFE), and Graciosa Island, Azores (GRW). Because a broad network of aerosol optical measurements already exists, this empirical method has the potential to provide data for model assimilation and validation of CCN processes on local to global scales.

2 Measurements

In-situ measurements of aerosol optical properties and CCN were conducted at the four ARM Climate Research Facility (ACRF) sites. The site location and measurement duration period are listed in Table 1 as well as the site aerosol optical properties of the scattering coefficient, backscatter fraction and single scattering albedo over the measurement period. SGP is a permanent facility and the other three sites, FKB, GRW and HFE, are a mobile facility with varying operations periods. Data sets are limited by the deployment period and instrument operation. Detailed information about each site is located on the ACRF web site at http://www.arm.gov/sites. SGP is located in an agricultural region in the central US. FKB is located in the Black Forest of Germany in

ACPD
10, 8995–9013, 2010

a valley with agriculture and surrounded by hills with coniferous forests. HFE is in the Anhui Province of China with mixed agricultural, pollution and dust aerosol sources. GRW is a remote marine site in the Atlantic Ocean with periodic local pollution from airport traffic and long-range transport from Europe.

The measurement configuration was similar at each site. Sheridan et al. (2001) gives a detailed description of the aerosol optical measurements at SGP. Sample air enters the system at ~800 lpm via a 10 m stack. The sample air splits between the five, 30 lpm sample lines. The sample for the optical measurements flows through an impactor which size segregates the aerosol between sub µm and sub 10 µm aerosol in 30 min intervals. A pickoff from one of the 30 lpm sample lines diverts a 500 ccm flow to the CCN instrument.

The properties of the aerosol total scattering (7–170°) and backscattering (90-170°) coefficients at 450, 550 and 700 nm radiation are measured with a TSI model 3563 integrating nephelometer. The aerosol light absorption coefficient was measured using a filter-based Radiance Research PSAP at 470, 528 and 660 nm radiation. Corrections based on light truncation in the nephelometer and aerosol scatter from the PSAP filter were performed (Anderson and Ogren, 1998; Bond et al.,1999). The 470 nm absorption coefficient was wavelength adjusted to 450 nm so that it would coincide with the scattering coefficient wavelength of the nephelometer.

The CCN at several supersaturations was measured using a DMT CCN counter (Roberts and Nenes, 2005). The percent supersaturation (%SS) of the instrument was stepped in 7 intervals every 30 min with 5 min at each setting in a pyramid form. The CCN instrument was serviced and calibrated at the beginning and end of each deployment for the mobile facility and bi-annually for the SGP site. The %SS in the CCN was calculated using a heat transfer and fluid dynamics model flow model (Lance et al., 2006). The model uses the calibrated temperature, pressure and flows in the instrument to calculate the %SS. Small variations in the %SS will arise from changes the in column thermal properties in the instrument. Rose et al. (2008) has an extensive discussion that compares model and salt calibration calculations of the instrument %SS

ACPD
10, 8995–9013, 2010

and uncertainty associated with thermal properties.

3 Empirical method

The empirical fit uses a power law, as derived by Twomey (1959), to parameterize the CCN activity spectra.

$$\mathrm{CCN}(\%\mathrm{SS}) = C(\%\mathrm{SS})^{k} \quad (1)$$

The fit used values of %SS in the range of 0.2 to 0.9, with variance of ±0.1% SS between sites. At higher %SS the k parameter decreases (Khvorostyanov and Curry, 2006) and below this range the uncertainty in the %SS increases (Rose et al., 2008). Fit parameters with poor goodness of fit chi-square values were rejected as they usually indicated noisy activation spectra or spikes in the data. The C and k fit parameters were then fit to linear correlations with the sub micron aerosol backscatter fraction and single scatter albedo at 450 nm as follows.

$$C/\sigma_{\mathrm{sp}}\ (450\ \mathrm{nm}) = m \cdot \mathrm{BSF}\ (450\ \mathrm{nm}) + b \quad (2)$$

$$k = m \cdot \mathrm{SSA}\ (450\ \mathrm{nm}) + b \quad (3)$$

Here, C is normalized to the submicron total angular scatter at 450 nm, σ_{sp} (450 nm), SSA (450 nm) is the aerosol sub µm single scattering albedo at 450 nm, m and b are the slope and offset of the linear correlations. The empirical fit calculates CCN by replacing the C and k fit parameters with the linear fits in Eqs. (2) and (3). In these fits BSF ranged between 0.08 and 0.18 and SSA was limited to 0.8 to 1.0. In order to screen for dust particles that may skew the fits, data with scattering Ångström exponents below 1.0 were eliminated.

The suitability of using aerosol optical measurements to predict CCN depends on the overlap between the critical aerosol size for activation to CCN and the aerosol scattering efficiency. The empirical fit maximizes this overlap by selecting sub µm

ACPD
10, 8995–9013, 2010

aerosol at the shortest wavelength of the nephelometer, 450 nm. The Mie scattering calculations of the aerosol backscatter fraction and scattering efficiency in Fig. 1 show the probable size range of the nephelometer measurements for different lognormal widths. The typical aerosol radius for CCN formation is about 20–100 nm (McFiggans et al., 2006), which is smaller than the sensitivity of the optical measurements. The comparison of CCN to aerosol optical properties assumes that the small mode aerosol are essentially a non-activating. There is much support from this study as well past field studies that small mode particles may have only a minimal contribution to CCN formation. From observations at all of the sites in this study the aerosol single scatter albedo decreases significantly with particle size (Fig. 2). Smaller particles tend to have a higher fraction of absorbing material that may limit their ability to act as CCN. A study of the size-dependent composition from several sites found that the organic fraction dominates the fine mode aerosol smaller than 100 nm diameter (McFiggans, et al., 2005). Another study by Ervens et al. (2007) found that the oxygenated organic fraction could be modeled as insoluble with respect to activation and still obtain good agreement with the measured CCN. As small aerosol likely have a high fraction of low solubility organics, the low sensitivity of the optical measurements in this size range may have a minimal effect on the empirical method of this study.

4 Results and discussion

The sites in this study are regional settings and as such represent aged aerosol of mixed composition. No one site has a characteristic single composition type to clearly distinguish it from the others. Instead the differences are subtle. Table 1 compares the average optical properties of the data used in the analysis between the four sites. The optical properties in Table 1 are only for sub µm particles at 450 nm and so ignore the coarse mode fraction. GRW and HFE have the smallest BSF and hence largest particles due to the influence of sea salt at GRW and probable dust at HFE. The likelihood of dust at HFE is supported from observation of construction in the region, the

ACPD
10, 8995–9013, 2010

presence of a local cement factory and coal mine as well as low Angstrom exponents and moderate to low hygroscopic growth factors typical of dust aerosol. The SSA at GRW is unexpectedly low at 0.88, which points to the influence of long-range transport of pollution aerosol as well as possible local pollution at the site despite extensive editing of short-duration data spikes to filter for local pollution. The data at GRW is biased toward times with higher aerosol loading, as the uncertainty of intensive properties at very low scattering and absorption signals was too high to include this data in the analysis. Both the HFE and FKB sites were influenced by frequent precipitation. The SSA was usually lower after a rain event as much of the highly soluble aerosol with higher SSA values may have been scavenged.

Figures 3 and 4 show the correlations between the power law fit parameters and the sub *um* aerosol backscatter fraction and single scattering albedo. The fits from SGP use data that span 0.2 to 0.8% SS in steps of 0.20, 0.41 0.60 and 0.80 ±0.01. Ranges of %SS for the other sites are given in Table 1. Because of conditions of high aerosol loading at HFE the lowest %SS value at ~0.2 was not used in the analysis. The CCN instrument may have insufficient water or too short of a sample residence time for the aerosol to activate under high aerosol concentrations and low %SS (DMT, 2009).

In order to show a direct correlation to the backscatter fraction and hence aerosol size, the power law parameter C is normalized to the aerosol scattering coefficient at 450 nm. This normalized parameter, C/σ_{sp} (450 nm), is the inverse aerosol scattering efficiency ($1/Q_{sp}$) in the case when 100% of the CN in the effective scattering size range activate to CCN. Figure 3 shows C/σ_{sp} (450 nm) increases as the aerosol size decreases at higher backscatter fractions. At these sites the aerosol scattering increases faster with aerosol size than CCN formation. This slope varies with measurement site and likely reflects differences in the size-dependent aerosol composition at each site. The slope in Figure 3 for GRW is significantly lower than the other three sites, which may reflect the aerosol sea salt composition as sea salt has a high scattering efficiency. The range of BSF at GRW was extended to 0.04 to accommodate the larger aerosol at this site and provide enough data for the fit calculation.

ACPD
10, 8995–9013, 2010

The k parameter indicates the steepness of the change in CCN concentration with %SS. Low values of k are typical of highly soluble aerosol such as sea salt and high k values of low-solubility aerosols. The range of k values (Table 1) and slope of k vs. SSA varies between sites. GRW has the lowest k values of 0.49 ±0.43 and FKB has the highest k values with 1.06±0.65. The range of SSA at HFE does not extend higher than 0.941. At this site absorbing aerosol is ubiquitous and may reflect a high organic fraction. The slope of k vs. SSA at both HFE and GRW is low. For these sites changes in the aerosol absorbing fraction or equivalent black carbon (EBC) have a weak influence on CCN formation. In these instances other compounds may moderate CCN activation. At GRW the aerosol composition may have a high enough sea salt fraction to weaken the influence of organics on CCN. At HFE dust may moderate the influence of EBC on CCN. The higher slopes of k vs. SSA at SGP and FKB alternatively indicate a strong influence of EBC and other organics on CCN formation.

Figure 5 shows the fit correlations to the measured CCN. All four sites exhibit good fits with r^2 correlation values of 0.66 or higher and slopes between 0.81 and 1.03. The goodness of the fit depends on both the ability of the power law fit parameters to represent the measured CCN as well as the correlation between the power law fit parameters, C and k, and the optical properties of BSF and SSA. For all of the fits the power law parameters under predict the measured CCN by 4 to 11%.

Figure 6 gives a clearer view of the reason for the low slopes and positive intercepts in the correlations. The empirical model over predicts CCN at low measured CCN values. This over prediction is highest for FKB and hence results in a lower slope in Fig. 5. At the lower aerosol number concentrations the uncertainty in the calculated SSA and BSF values are higher. Another contributing factor to this uncertainty is the nonlinearity of the correlation between the k fit parameter and SSA, particularly at low SSA values. Despite these limitations the empirical fit is able to predict the measured CCN within ±50% at the higher concentrations using only the aerosol optical properties as proxies for aerosol composition and size.

ACPD
10, 8995–9013, 2010

5 Summary and conclusions

An empirical model uses the aerosol optical properties to predict the measured CCN concentration as a function of percent super saturation. The aerosol backscattering fraction and single scatter albedo act as proxies for the aerosol size and composition in the model. Relatively good agreement was found between the predicted and measured CCN values with higher uncertainties at low CCN concentrations.

The fit parameters varied with aerosol type and region. The slope of C/σ_{sp} (450 nm) vs. BSF was higher at continental sites and lower at a marine site. This parameter represents the inverse size-dependent scattering efficiency of the CCN and is therefore expected to be high for organic aerosol with low scattering efficiency and lower for sea salt, which has a high scattering efficiency.

The second fit parameter is the slope of k vs. SSA and signifies the relative growth of CCN with %SS as a function of the aerosol absorption or EBC content. For combustion aerosol the BC and total organic carbon content usually covary and the second parameter would be an indication of the effect of organic aerosol on CCN formation. This may not be the case for noncombustion organic aerosol. This slope of k vs. SSA varied between continental sites, a marine site and a site influenced by dust. At the marine site changes in the SSA had a weak influence on k and may indicate that a highly hygroscopic compound like sea salt can moderate the influence of less hygroscopic species like BC. Having even a small fraction of sea salt in the aerosol may be enough for the aerosol to activate even at low %SS, especially if the aerosol is relatively large as was the case at GRW. The slope of k vs. SSA was also low at HFE, which could be a factor of dust moderating the aerosol activation as well as high scatter and uncertainty in the data.

This study is a first step in a process to better predict CCN concentration as a function of %SS from the aerosol optical properties. Further analysis includes well-defined fit parameters for each aerosol type and region. Having well-defined fit parameters for an aerosol type will entail analysis of seasonal trends of the fits and comparison to

ACPD
10, 8995–9013, 2010

size-dependent aerosol composition to better quantify the fit parameters with aerosol type.

Acknowledgements. I wish to acknowledge the ACRF support staff and technicians, especially Mike Alsop and Pat Dowell. I also thank Allison McComisky for helpful discussions.

References

Anderson, T. L. and Ogren, J. A.: Determining aerosol radiative properties using the TSI 3563 integrating nephelometer, Aerosol Sci. Tech., 29, 57–69, 1998.

Andreae, M. O.: Correlation between cloud condensation nuclei concentration and aerosol optical thickness in remote and polluted regions, Atmos. Chem. Phys., 9, 543–556, 2009, http://www.atmos-chem-phys.net/9/543/2009/.

Bond, T. C., Anderson, T. L., and Campbell, D.: Calibration and intercomparison of filter-based measurements of visible light absorption by aerosols, Aerosol Sci. Tech., 30, 582–600, 1999.

DMT, Cloud Condensation Nuclei Counter Operator Manual, DOC-0086 Rev G-1, Droplet Measurement Technologies, Inc., p. 107, 2009.

Ervens, B., Cubison, M. J., Andrews, E., Feingold, G., Ogren, J. A., Jimenez, J. L., Quinn, P. K., Bates, T. S., Wang, J., Zhang, Q., Coe, H., Flynn, M., and Allan, J. D.: CCN predictions using simplified assumptions of organic aerosol composition and mixing state: a synthesis from six different locations, Atmos. Chem. Phys. Discuss., 9, 21237–21256, 2009, http://www.atmos-chem-phys-discuss.net/9/21237/2009/.

Ghan, S., Chuang, C., Easter, R., and Penner, J.: A parameterization of cloud droplet nucleation. 2, Multiple aerosol types, Atmos. Res., 36, 39–54, 1995.

Ghan, S. J., Rissman, T. A., Elleman, R., Ferrare, R. A., Turner, D., Flynn, C., Wang, J., Ogren, J., Hudson, J., Jonsson, H. H., VanReken, T., Flagan, R. C., and Seinfeld, J. H.: Use of in situ cloud condensation nuclei, extinction, and aerosol size distribution measurements to test a method for retrieving cloud condensation nuclei profiles from surface measurements, J. Geophys. Res., 111, D05S10, doi:10.1029/2004JD005752, 2006.

Good, N., Topping, D. O., Allan, J. D., Flynn, M., Fuentes, E., Irwin, M., Williams, P. I., Coe, H., and McFiggans, G.: Consistency between parameterisations of aerosol hygroscopicity and CCN activity during the RHaMBLe Discovery cruise, Atmos. Chem. Phys. Discuss., 9,

22659–22692, 2009, http://www.atmos-chem-phys-discuss.net/9/22659/2009/.
Khvorostyanov, V. I. and Curry, J. A.: Aerosol size spectra and CCN activity spectra: Reconciling the lognormal, algebraic, and power laws, J. Geophys. Res., 111, D12202, doi:10.1029/2005JD006532, 2006.
Lance, S., Medina, J., Smith, J. N., and Nenes, A.: Mapping the operation of the DMT continuous flow CCN counter, Aerosol Sci. Tech., 40(4), 242–254, 2006.
McFiggans, G., Alfarra, M. R., Allan, J. D., Bower, K. N., Coe, H., Cubison, M., Topping, D. O., Williams, P. I., Decesari, S., Fac- chini, M. C., and Fuzzi, S.: Simplification of the representation of the organic component of atmospheric particulates, Faraday Discuss., 130, 1–22, doi:10.1039/b419435g, 2005.
McFiggans, G., Artaxo, P., Baltensperger, U., Coe, H., Facchini, M. C., Feingold, G., Fuzzi, S., Gysel, M., Laaksonen, A., Lohmann, U., Mentel, T. F., Murphy, D. M., O'Dowd, C. D., Snider, J. R., and Weingartner, E.: The effect of physical and chemical aerosol properties on warm cloud droplet activation, Atmos. Chem. Phys., 6, 2593–2649, 2006, http://www.atmos-chem-phys.net/6/2593/2006/.
Petters, M. D. and Kreidenweis, S. M.: A single parameter representation of hygroscopic growth and cloud condensation nucleus activity, Atmos. Chem. Phys., 7, 1961–1971, 2007, http://www.atmos-chem-phys.net/7/1961/2007/.
Petters, M. D., Wex, H., Carrico, C. M., Hallbauer, E., Massling, A., McMeeking, G. R., Poulain, L., Wu, Z., Kreidenweis, S. M., and Stratmann, F.: Towards closing the gap between hygroscopic growth and activation for secondary organic aerosol – Part 2: Theoretical approaches, Atmos. Chem. Phys., 9, 3999–4009, 2009, http://www.atmos-chem-phys.net/9/3999/2009/.
Roberts, G. and Nenes, A.: A continuous-flow streamwise thermal- gradient CCN chamber for atmospheric measurements, Aerosol Sci. Tech., 39(3), 206–221, 2005.
Rose, D., Gunthe, S. S., Mikhailov, E., Frank, G. P., Dusek, U., Andreae, M. O., and Pöschl, U.: Calibration and measurement uncertainties of a continuous-flow cloud condensation nuclei counter (DMT-CCNC): CCN activation of ammonium sulfate and sodium chloride aerosol particles in theory and experiment, Atmos. Chem. Phys., 8, 1153–1179, 2008, http://www.atmos-chem-phys.net/8/1153/2008/.
Sheridan, P. J., Delene, D. J., and Ogren, J. A.: Four years of continuous surface aerosol measurements from the Department of Energy's Atmospheric Radiation Measurement Pro-

gram Southern Great Plains Cloud and Radiation Testbed site, J. Geophys. Res., 106(D18), 20735–20747, 2001.

Shinozuka, Y., Clarke, A. D., DeCarlo, P. F., Jimenez, J. L., Dunlea, E. J., Roberts, G. C., Tomlinson, J. M., Collins, D. R., Howell, S. G., Kapustin, V. N., McNaughton, C. S., and Zhou, J.: Aerosol optical properties relevant to regional remote sensing of CCN activity and links to their organic mass fraction: airborne observations over Central Mexico and the US West Coast during MILAGRO/INTEX-B, Atmos. Chem. Phys., 9, 6727–6742, 2009, http://www.atmos-chem-phys.net/9/6727/2009/.

Solomon, S., Qin, D., Manning, M., Alley, R. B., Berntsen, T., Bindoff, N. L., Chen, Z., Chidthaisong, A., Gregory, J. M., Hegerl, G. C., Heimann, M., Hewitson, B., Hoskins, B. J., Joos, F., Jouzel, J., Kattsov, V., Lohmann, U., Matsuno, T., Molina, M., Nicholls, N., Overpeck, J., Raga, G., Ramaswamy, V., Ren, J., Rusticucci, M., Somerville, R., Stocker, T. F., Whetton, P., Wood, R. A., and Wratt, D., Technical Summary, in: Climate Change 2007: The Physical Science Basis. Contribution of Working Group I to the Fourth Assessment Report of the Intergovernmental Panel on Climate Change, edited by: Solomon, S., Qin, D., Manning, M., Chen, Z., Marquis, M., Averyt, K. B., Tignor, M., and Miller, H. L., Cambridge University Press, Cambridge, United Kingdom and New York, NY, USA, 2007.

Svenningsson, B., Rissler, J., Swietlicki, E., Mircea, M., Bilde, M., Facchini, M. C., Decesari, S., Fuzzi, S., Zhou, J., Mønster, J., and Rosenørn, T.: Hygroscopic growth and critical supersaturations for mixed aerosol particles of inorganic and organic compounds of atmospheric relevance, Atmos. Chem. Phys., 6, 1937–1952, 2006, http://www.atmos-chem-phys.net/6/1937/2006/.

Twomey, S.: The nuclei of natural cloud formation.II The supersaturation in natural clouds and the variation of cloud droplet concentration, Pure Appl. Geophys., 43, 243–249, 1959.

Table 1. Field site name, location, date of operation, range of % super saturation, average of aerosol sub µm scattering coefficient (σ_{sp}), backscatter fraction, single scatter albedo at 450 nm and power law k fit parameter. Values in parentheses are (±1 std dev.).

Site	lon. lat.	Date	%SS range	σ_{sp}	BSF	SSA	k
SGP	36°36′ N, 97°29′ W	10 Feb–20 May 2009	0.19–0.82	47 (51)	0.12 (0.02)	0.92 (0.04)	0.73 (0.26)
FKB	48°32′ N, 08°23′ E	31 May–6 Dec 2007	0.26–0.83	51 (38)	0.12 (0.02)	0.88 (0.04)	1.06 (0.65)
HFE	32°33′ N, 116°46′ E	26 Jul–23 Aug 2008	0.40–0.88	118 (68)	0.10 (0.01)	0.89 (0.03)	0.76 (0.33)
GRW	39°5′ N, 28°1′ W	20 Apr–27 Sep 2009	0.21–0.86	11 (8)	0.09 (0.02)	0.88 (0.06)	0.43 (0.42)

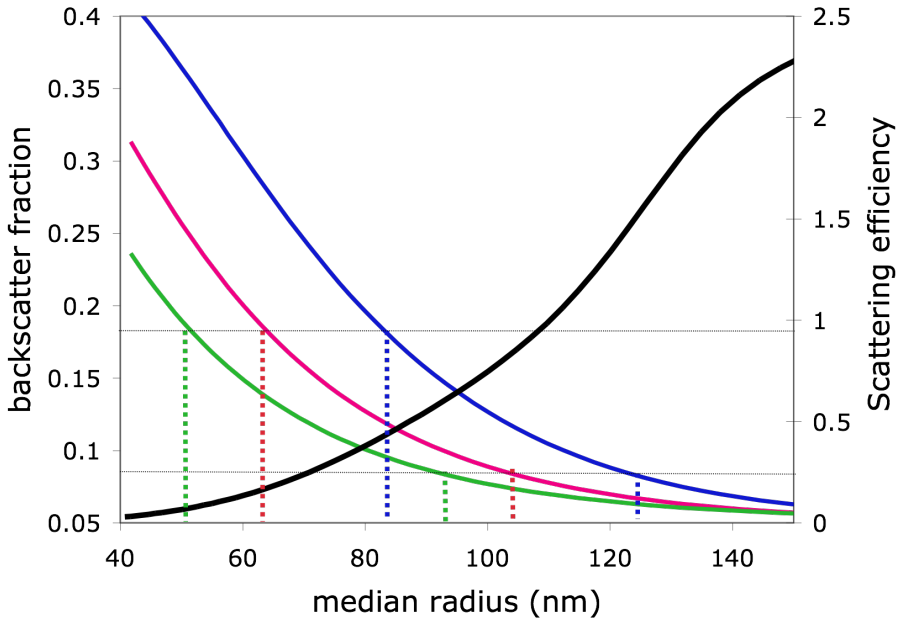

Fig. 1. Mie calculations of the aerosol scattering efficiency (black line), and backscatter fraction at three lognormal distribution widths of $s = 1.4$ (blue), 1.5 (red) and 1.6 (green). The dashed lines show the range of backscatter values used in this study.

ACPD
10, 8995–9013, 2010

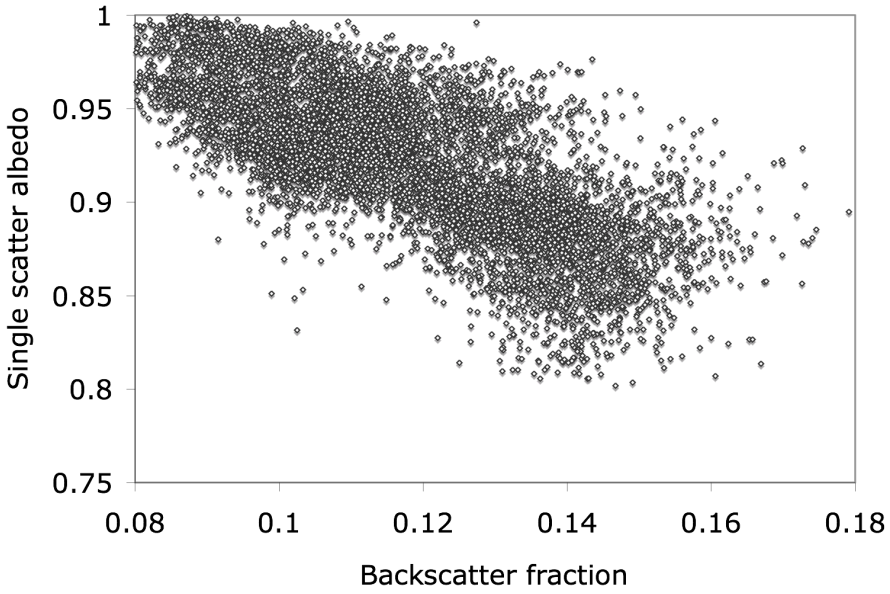

Fig. 2. Single scatter albedo vs backscatter fraction at 450 nm. Data is from SGP.

ACPD
10, 8995–9013, 2010

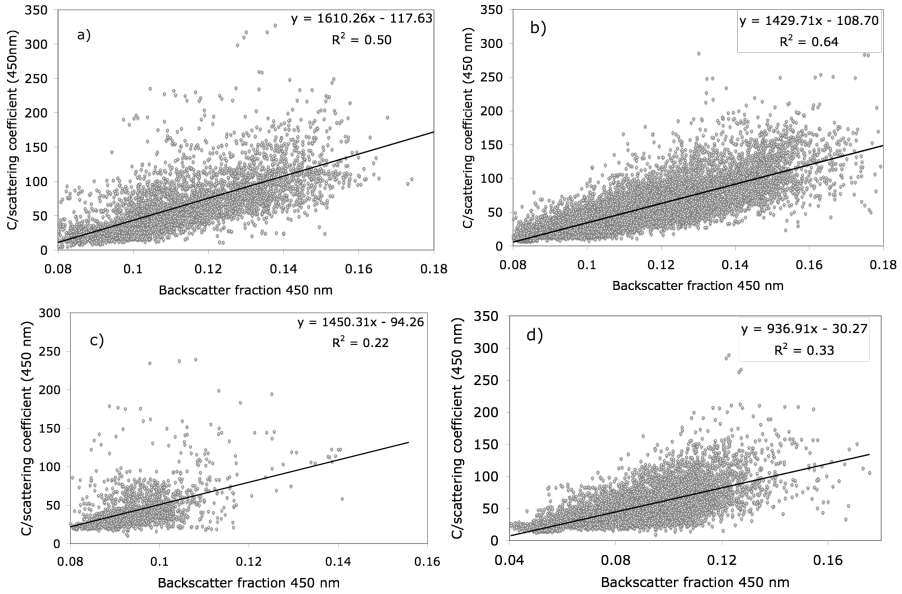

Fig. 3. Graphs of C/scattering coefficient vs backscatter fraction at 450 nm for **(a)** SGP **(b)** FKB **(c)** HFE and **(d)** GRW.

ACPD
10, 8995–9013, 2010

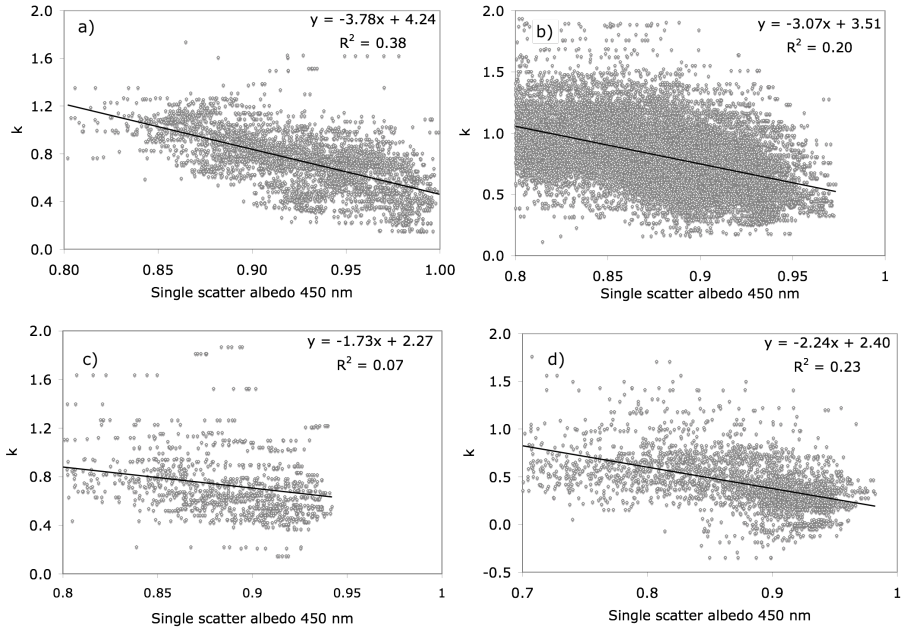

Fig. 4. Graphs of *k* parameter vs. single scatter albedo at 450 nm for **(a)** SGP **(b)** FKB **(c)** HFE and **(d)** GRW.

ACPD
10, 8995–9013, 2010

Empirical predictions of CCN from aerosol optical properties

A. Jefferson

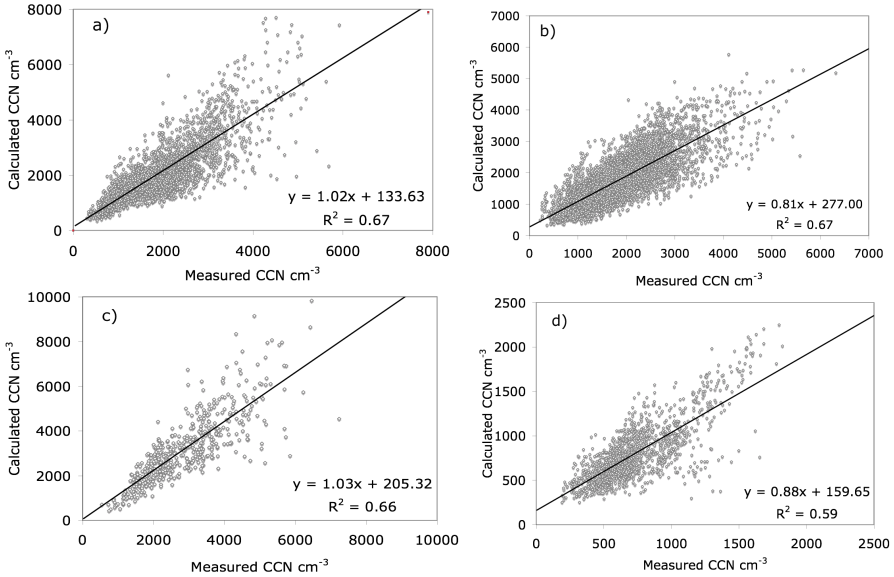

Fig. 5. Correlations of calculated and measured CCN for **(a)** SGP, **(b)** FKB, **(c)** HFE and **(d)** GRW.

ACPD
10, 8995–9013, 2010

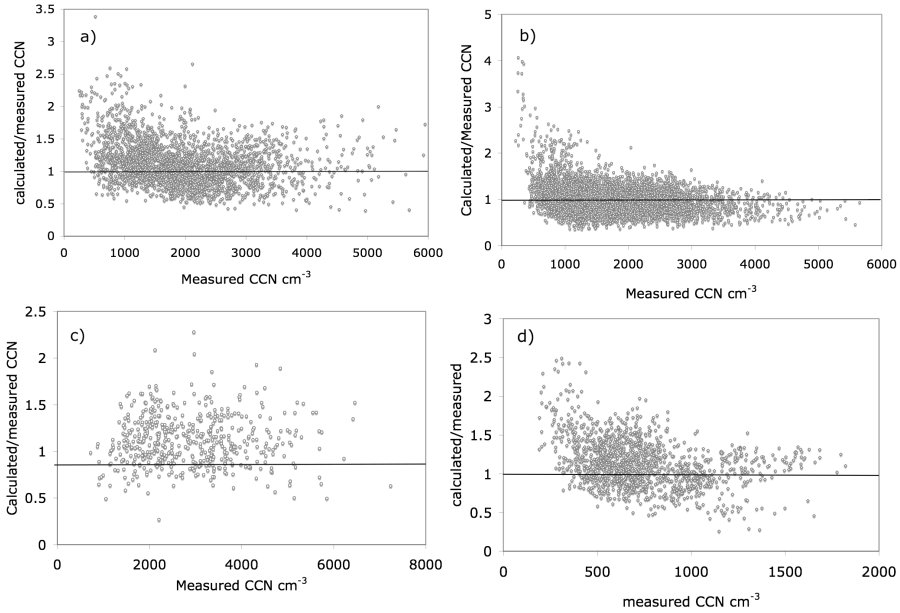

Fig. 6. Correlations of calculated/measured CCN and measured CCN for **(a)** SGP, **(b)** FKB, **(c)** HFE and **(d)** GRW.

ACPD
10, 8995–9013, 2010